Towards Membrane-Free Amperometric Gas Sensors: A Microelectrode Array Approach

Journal:	*Analytical Chemistry*
Manuscript ID:	ac-2010-006359.R2
Manuscript Type:	Article
Date Submitted by the Author:	26-Apr-2010
Complete List of Authors:	Huang, Xing-Jiu; University of Oxford, Department of Chemistry Aldous, Leigh; University of Oxford, Department of Chemistry O'Mahoney, Aoife; University of Oxford, Department of Chemistry del Campo, Francisco Javier; Consejo Superior de Investigaciones Científicas, CSIC, Instituto de Microelectrónica de Barcelona, IMB-CNM Compton, Richard; University of Oxford, Department of Chemistry

Towards Membrane-Free Amperometric Gas Sensors: A Microelectrode Array Approach

Xing-Jiu Huang,[†] Leigh Aldous,[†] Aoife M. O'Mahony,[†] F. Javier del Campo,[‡] and Richard G. Compton[†,*]

[†] Department of Chemistry, Physical and Theoretical Chemistry Laboratory, University of Oxford, South Parks Road, Oxford OX1 3QZ, United Kingdom,

[‡] Instituto de Microelectrónica de Barcelona, CNM (CSIC), Campus de la Universidad Autónoma de Barcelona, Bellaterra 08193, Spain

Submitted to *Analytical Chemistry*

Keywords: Microarray, Ionic Liquids, Carbon Nanotubes, Electroanalysis, Oxygen detection

[*]Author to whom all correspondence should be addressed

E-mail: richard.compton@chem.ox.ac.uk

Tel.: +44 (0) 1865 275 413

Fax.: +44 (0) 1865 275 410

Abstract

Room temperature ionic liquids (RTILs) have been applied to a microelectrode array, and been demonstrated to form effective, membrane-free amperometric gas sensors. Determining the RTIL $[P_{6,6,6,14}][FAP]$ as the most appropriate choice for extended use, the amperometric quantification of oxygen has been demonstrated. The response of the sensor was quantified by both cyclic voltammetry and chronoamperometry. A range of O_2 contents (2 to 13 % v/v) and RTIL layer thicknesses (from *ca.* 6 to 125 µm) have been investigated. The combination of microelectrode array and RTIL, as well as the absence of membrane and volatile solvent, results in an elegant, easy to calibrate gas sensor with potential utility in standard and non-standard conditions.

Introduction

Amperometric gas sensors were originally developed over the last five decades to allow the measurement of gases such as oxygen and carbon dioxide in the context of physiological investigations. In essence these 'Clark electrodes' take the form of macroelectrodes covered by a gas permeable membrane which retains a layer of electrolyte, usually aqueous, into which the gas dissolves before undergoing electrolysis at the electrode. This generates a current which reflects the presence of the target molecule in the gas phase.[1] Subsequent developments have utilised microelectrodes and/or non-aqueous solvents resulting in sensors for a huge range of gases (O_2, O_3, CO, CO_2, SO_2, NO, NO_2, Cl_2, NH_3, *etc*.) which are commercially available through the manufacturing companies, such as Honeywell,[2] Alphasense,[3] City Technology,[4] Draeger,[5] *etc.*

Commercially available gas sensors are relatively cheap, easy to use, sensitive and selective. That said, some limitations on their operation arise for two reasons. First, the sensors are prone to drying out; the electrolyte solvent evaporates and the device fails. Second, the use of microelectrodes or microelectrode arrays at steady-state establishes concentration gradients for the target species between the electrode surface and the internal surface of the membrane. As a consequence of the encroachment of the electrodes diffusion layer on the membrane, the sensor becomes sensitive to the properties of the latter (thickness, age, gas solubility, gas diffusivity, *etc.*), as well as the variation of all of these properties with temperature if variable temperature is

desired, as it usually the case.

It has been proposed that considerable benefits might arise through the use of room temperature ionic liquids (RTILs) as solvents in amperometric gas sensors of the Clark type.[6] In the past few years extensive investigations have been carried out on RTILs; key physical properties relevant to the work carried out here are their typically large electrochemical windows, inherent conductivity, chemical robustness, thermal stability, large liquidus range and their low or negligible volatility.[7]

In the context of gas sensors, the low or negligible volatility of some RTILs should reduce the likelihood of sensor failure through evaporative loss of the electrolyte. Moreover, because of the relatively low vapour pressure demonstrated by many RTILs, it may become possible to eliminate the need for a membrane. That is to say that the layer of RTIL covering an electrode assembly could serve as the sensing unit. In this way the device response would no longer reflect membrane properties but just these of the RTIL and the electrode geometry selected for use. The avoidance of a membrane thus eliminates some need for device calibration and greatly simplifies the temperature response of the sensor. The potential utility of these low volatitilty Clark-type sensors in non-standard conditions (*e.g.* elevated temperature, low pressure) or in the presence of sensitive materials (*e.g.* controlled humidity conditions or in proximity to pyrophoric materials) is also apparent.

Considerable research has taken place into the electrochemical characteristics of O_2 in RTILs.[8-19] This has largely consisted of fundamental research, investigating important parameters such as reduction and re-oxidation processes,[10,12,16] chemical reactivity and RTIL stability [12,14,16,18,19] and fundamental electrochemical constants.[8,9,11,13,15] Often these experiments were carried out under defined equilibrated conditions and using single micro- or macroelectrodes. Microelectrode arrays can offer the improved signal-to-noise ratio and other characteristics associated with single microelectrodes, while also providing the larger current densities and signal outputs required for commercial amperometric sensing devices.[20]

In the context of gas sensors, Buzzeo *et al.* investigated relatively deep (*e.g.* semi-infinite) layers of RTILs on a single microelectrode, but found that the resulting small limiting currents and slow response limited their applicability under standard conditions with respect to traditional Clark cells.[6] Wang *et al.* investigated solid-state sensors which could be used to quantify O_2 in dry gas streams, prepared from RTILs supported by polyethylene membrane-coated electrodes.[21,22] Jin *et al.* prepared a RTIL high-temperature sensor for organic vapours, by depositing thin layers of RTILs on a quartz crystal microbalance and relating weight change to dissolution of the vapours into the RTIL.[23] Layers of RTIL have also been investigated for the gas-phase preconcentration and electrochemical quantification of phenols [24] and nitroaromatics.[25] In the latter study the reduction peak of O_2 was

used as an internal reference.

In this paper we show that a microarray covered in a layer of RTIL can operate as a membrane-free amperometric O_2 sensor. A variety of RTIL film thicknesses (from *ca.* 6 µm to *ca.* 125 µm) were investigated, with both larger current responses and more rapid response times observed with thinner films. The described system corresponds to a significantly simplified response to O_2 compared to membrane-based sensors, as well as allowing the possible application of Clark-type sensors in situations where volatiles electrolytes are not suitable.

EXPERIMENTAL SECTION

Chemical Reagents. Tris(n-hexyl)tetradecylphosphonium trifluorotris(penta-fluoroethyl)phosphate ($[P_{6,6,6,14}][FAP]$, high purity) was kindly donated by Merck KGaA and used as received. Ferrocene (Fc, Aldrich, 98%) and acetonitrile (Fischer Scientific, dried and distilled, >99.99%) were used as received without further purification. Pure oxygen and nitrogen gas (BOC, Guildford, Surrey, UK) were used for electrochemical experiments as described below. All the solutions were vigorously degassed with an air extraction pump (Edwards high vacuum pump, model ES 50) until oxygen was not electrochemically detectable.[9,11] All experiments were carried out at room temperature.

A solution of 10 mM Fc in $[P_{6,6,6,14}][FAP]$ was prepared by dissolving appropriate quantities of the viscous RTIL and solid Fc in acetonitrile, removing the acetonitrile under vacuum and then drying [26] the resulting RTIL/Fc solution under high vacuum for 24 hrs.

Activation of the chips. Prior to cyclic voltammetry measurements, the working electrodes in the recessed Au microdisc array were first activated in 0.1 M KCl solution by a potential step method. A Pt wire served as counter electrode and a SCE was used as reference electrode. The potential was stepped to -2 V *vs.* SCE and then back to 0 V, holding at each potential for 5 s. This was repeated five times, in order to obtain an electrochemically cleaned, reproducible electrode surface.

Apparatus. Cyclic voltammetry (CV) was performed using a type II μAutolab (Eco Chemie, Utrecht, Netherlands), which was interfaced with a PC using GPES (version 4.9) software for Windows. For electrochemical experiments carried out on the chip, the working electrode was the recessed microdisc array (Connector 2), together with a large auxiliary electrode counter electrode (Connector 1), and a smaller auxiliary reference electrode (Connector 3). Connector 4 (ring electrodes) was not used in this work. Different amounts of $[P_{6,6,6,14}][FAP]$/Fc were dropped onto the chip using an adjustable micropipette (Eppendorf, 0.1-2.5 µl). The activated chip was housed in a glass "T-cell" [9] specially designed to control the gaseous environment.

Prior to the addition of gases, the complete cell arrangement was placed under vacuum (Edwards high vacuum pump, model ES 50) until the baseline showed no trace of atmospheric oxygen (typically ~60 min). Oxygen and nitrogen were introduced to the electrochemical cell in desired ratios using a Wösthoff triple gas-mixing pump (Bochum), accurate to ±1%. Gas mixtures were passed through the cell for at least 30 min prior to starting a set of experiments (unless otherwise stated in the text) in order to ensure the system was equilibrated.

Images of the microdisc array surface were captured with a Sony XC-999P CCD camera attached to an optical OMVPAR microscope. The microdisc electrode array was also investigated by confocal microscopy using a PLµ non-contact confocal imaging profiler system attached to a Nikon microscope using a 50x magnification lens, and controlled using PLµ proprietary software (Sensofar, Spain).

RESULTS AND DISCUSSION

Chip fabrication

The recessed microdisc-ring devices were produced on silicon wafers using standard fabrication techniques. The fabrication process comprised two metallisations, several oxidation and deposition steps, three photolithographic steps and a combination of dry and wet etching steps. A similar process has been described elsewhere [27] but it is illustrated in Figure 1 and a short summary will be given here for convenience.

A 1 µm thick thermal oxide layer was grown on 4-inch silicon wafers to provide electrical insulation to the microelectrode structures (Figure 1, A.2). Next, a metal tri-layer consisting of Ti (25nm), Ni (25nm) and Au (125nm) was deposited by sputtering (Figure 1, A.3). The titanium layer acted as adhesion promoter for the other metals, and nickel was used as diffusion barrier. The wafer was subject to the first photolithographic step after this metallisation (Figure 1, A.4 and B.1) to define the metal regions that would later make the bottom level microelectrodes and their contact pads.

Next, a silicon oxide layer was deposited by Plasma-enhanced chemical vapor deposition (Figure 1, A.5). This layer separates the metal levels featuring the microdiscs below and the microrings above in the finished devices. The thickness of this oxide layer was close to 1 µm, and its deposition was followed by the second metallisation (Figure 1, A.6), which was done to the same specifications as the first one.

The second photolithographic step defined the top level electrode areas and their contact pads, again using a clear field mask (Figure 1, B.2). This step also defined the geometry of the underlying microdisc electrodes and their arrangement in the array.

Next, the wafers were passivated by *ca.* 200nm of silicon oxide and *ca.* 400 nm of silicon nitride (Figure 1, A.8). The two dielectric layers, which define the microrings on the top metal layer, the microdiscs in the bottom level and the contact pads to the microelectrodes in both levels, were patterned through the third photolithography step (Figure 1, A.9 and B.3) and the combination of dry etching by reactive ion etching (RIE) and wet etching in buffered HF. RIE was used to etch the top silicon nitride-silicon oxide layer and pattern the microrings (Figure 1, A.10). Then the wafers were transferred to a bath containing Sioetch® MT 06/01 solution (BASF) where the intermediate silicon oxide was removed (Figure 1, A.11). The fabrication was complete after the excess resin was stripped from the wafers. Last, the wafers were diced into individual chips, which were subsequently mounted, wire-bonded and encapsulated on suitable PCB boards.

Physical layout and characterisation of the chip

Figure 2A displays an enlarged diagram of the general layout of the chip (real dimensions 4 mm x 4 mm). The chip consists of a large outer Au counter electrode, surrounding an Au *quasi*-reference electrode and a central array consisting of 80 (10 by 8) Au microelectrodes. Figure 2B displays a representative optical microscopy image of part of the regular array. The centre-to-centre distance between adjacent

microdiscs is 150 μm.

The microarray was further characterized by confocal microscopy. Figure 2C displays a 3-D confocal microscopy image, focusing upon a single recessed microdisc electrode. Figure 2D displays the height profile (please note scale on the x- and y-axis) obtained by a 2-D scan passing along the dotted white line in Figure 2C, demonstrating that the recessed areas containing the microelectrodes are *ca.* 12 μm in diameter and *ca.* 1.6 μm deep.

Selection of a suitable ionic liquid

An enormous variety of RTILs are available, many of which possess the characteristics required for a versatile, long-lived membrane-less sensor (*e.g.* liquid at a wide range of temperatures, conductive and essentially non-volatile). However, surface tension measurements of a range of RTILs on the upper material of the microarray (Si_3N_4) are, to the best of our knowledge, not available. As such, qualitative testing was required. After testing $[C_2mim][NTf_2]$, $[N_{6222}][NTf_2]$ and $[C_4mPyrr][NTf_2]$, it was found that varying amounts of each were required in order to form a complete film over the entire surface of the chip (as opposed to a single droplet in one corner that did not extend the width of the chip). Additionally, it was found that many of the films were unstable over a period of hours, gradually retreating to form small discontinuous droplets on the array surface, which is attributed to uptake of atmospheric moisture altering the RTILs surface tension.

The RTIL $[P_{6,6,6,14}][FAP]$ was selected as it is one of the most hydrophobic

RTILs reported.[28] This RTIL was found to readily form thin films on the hydrophobic surface of the microarray, and due to its known low water uptake [26,28] these films were visually observed to be uniformly distributed on the surface of the array even after *ca.* 72 hours. It was for these reasons, as well as the RTILs aprotic nature and wide electrochemical window,[26,29] that it was selected in order to demonstrate proof of concept. It can be envisioned that subsequent surface optimisation (leading to thinner RTIL layers) and RTIL optimisation (*e.g.* RTILs less viscous that the 464 cP reported [30] at 25°C for $[P_{6,6,6,14}][FAP]$) could further exceed the excellent results reported in this paper for $[P_{6,6,6,14}][FAP]$.

Voltammetry in the presence of oxygen

Figure 3 displays CVs recorded at 0.1 V s^{-1} for a layer of 0.2 µL $[P_{6,6,6,14}][FAP]$ (*ca.* 12.5 µm in depth) on the recessed Au microdisc array. A clean baseline was observed in 100 % N_2, while a clear reduction peak was observed starting at *ca.* -1.2 V for a 3.5% O_2 / 96.5% N_2 mixture. The reduction peak approached steady state conditions, as expected for a microelectrode array, and corresponds to the one-electron reduction of oxygen to superoxide (equation (1)). After reversing the scan an oxidation peak was observed at *ca.* -1.14 V. This corresponds to the reoxidation of the accumulated superoxide to oxygen, confirming [14] that the electrochemically generated superoxide is relatively stable and chemically reversible in this system.

$$O_2 + e^- \rightarrow O_2^{\bullet -} \quad (1)$$

The system was further investigated as a function of scan rate. The $[P_{6,6,6,14}][FAP]$ was prepared to contain 10 mM ferrocene (Fc) as an internal reference. Figure 4 displays a scan rate study for 2.3 % v/v O_2 and 97.7 % v/v N_2 at a film thickness of 125 µm (2 µL RTIL). The oxidation and subsequent reduction of Fc can clearly be observed at *ca.* +0.2 V, while the reduction of O_2 appears at *ca.* -1.2 V. At all scan rates (0.1, 0.4 and 1 V s^{-1}) Fc displays peaks corresponding to transient behaviour, while O_2 displays a steady state reduction wave at 0.1 V s^{-1} which begins to approach transient behaviour as the scan rate is increased. The diffusion coefficient of O_2 and Fc differ by almost two degrees of magnitude in $[P_{6,6,6,14}][FAP]$ (*e.g.* $D_{O_2} = 61\times10^{-11}$ m^2 s^{-1} [14] and $D_{Fc} = 0.86\times10^{-11}$ m^2 s^{-1} [31]), and therefore the observed behaviour is what is expected for the system. Equation (2) highlights the conditions a system has to fulfill in order for the analyte to reach steady state behaviour at a specific scan rate, *v*, at a microelectrode of radius r_d.[32]

$$\upsilon < \frac{RTD}{nFr_d^2} \qquad (2)$$

Inputting the physical values into equation (1), Fc requires $v << 0.007$ V s^{-1} to generate steady-state behaviour, while O_2 requires $v << 0.5$ V s^{-1}, which is consistent with the observed scans.

Effect of RTIL layer thickness

Figure 5 displays scans of $[P_{6,6,6,14}][FAP]$ containing 10 mM Fc, at four different RTIL layer thicknesses (*ca.* 6, 30, 95, and 125 µm) after being exposed to a gas mixture containing 2.3 % v/v O_2 and 97.7 % v/v N_2. It can clearly be observed that as the thickness of the layer decreases, the peak oxidation current for Fc decreases while the limiting reduction current for O_2 actually increases. These apparently contrary observations are rationalized below.

Electrolysis of a dissolved species at an electrode creates a concentration gradient, triggering diffusion of the species from bulk solution and establishing a diffusion layer extending out from the electrode surface. The size of the diffusion layer, δ, can be approximated by equation (3),

$$\delta = 6\sqrt{Dt} \quad (3)$$

where t is electrolysis time and D is the electrolysed species diffusion coefficient. Assuming t = 3 s (*e.g.* time to scan from +0.1 to +0.4 V at 0.1 Vs^{-1}) and using the previously discussed values of D, δ_{Fc} = *ca.* 30 µm and δ_{O_2} = *ca.* 260 µm. Therefore, this implies that for all of the thicknesses shown in Figure 6, O_2 should display thin layer behaviour (*e.g.* a reduction peak rather than a steady-state wave), as the diffusion layer for O_2 will extend the entire depth of the RTIL (largest RTIL thickness *ca.* 125 µm, electrode-to-electrode separation in the array *ca.* 145 µm), and the bulk solution of O_2 in RTIL required to maintain steady state voltammetry will not persist throughout the timescale of the scan. Conversely, the diffusion layer for Fc is

relatively small in $[P_{6,6,6,14}][FAP]$, and an undisturbed bulk solution of Fc should persist on the timescale of the scan for RTIL thicknesses of *ca.* 30, 95, and 125 μm, such that the Fc oxidation peaks should in fact be visually identical in Figure 6 at these three thicknesses.

The observed behaviour of Fc was rationalised by a control experiment. A solution of *ca.* 2 mM Fc in $[P_{6,6,6,14}][FAP]$ was prepared, and 0.5 μL deposited on the surface of the microarray. In the case of both continuous cyclic voltammetric scans and periodic scans, the peak current response for both Fc oxidation and Fc^+ reduction were observed to decrease, therefore the decrease did not correlate with either the number of scans conducted in the system nor O_2 reduction. In the case of N_2 gas flowing continuously at *ca.* 500 mL min^{-1} and continuous scanning at 100 mV s^{-1}, the voltammetric response of Fc decreased in a linear manner by *ca.* 0.9 pA s^{-1}. Similar observations have been noted during the *in vacuo* electrochemistry of Fc dissolved in $[C_2mim][NTf_2]$ [33] and $[C_4mim][NTf_2]$,[34] and the decrease in peak size in the control experiment can therefore be related to the evaporation of Fc into the N_2 gas flow from the RTIL solution. It should be noted that the room temperature sublimation of solid Fc under a constant N_2 gas flow has previously been reported in the literature.[35]

The evaporation of Fc also explains the changes in Fc voltammetry with changing film thickness in Figure 6. Each sample was exposed to a flow of gas for 30 min prior to scanning. During this 30 min equilibration period each sample is assumed to have lost an equivalent amount of Fc (in the order of ng). However, the effect of

this loss on the decrease in bulk Fc concentration will be directly proportional to the volume of IL present (and therefore film thickness). Therefore, the observed differences in Figure 5 are not an effect of the layer thickness on the voltammetry, and instead correspond to each sample having a different bulk Fc concentration at the time of the scan.

The reduction of O_2 to superoxide is clearly observed as steady-state waves for all RTIL thicknesses, with the limiting current increasing as the RTIL layer thickness decreases. As discussed above, the diffusion layer for O_2 is expected to extend to the edge of the RTIL layer, and the observed behaviour therefore corresponds to the body of gas flowing over the RTIL acting as a well mixed, bulk supply of O_2 on the time scale of the scan. This constant flux of O_2 allows the observed steady-state behaviour in Figures 4 and 5, despite the limited quantity of RTIL. Furthermore, the entire RTIL layer acts as the diffusion layer, and the thinner the layer of RTIL the steeper the O_2 concentration gradient (between electrode and gas phase). As predicted by Fick's 1st Law of Diffusion, a corresponding increase in the flux of O_2 from the gas phase to the electrode is observed as the gradient in increased, leading to the enhanced current demonstrated experimentally in Figure 5.

Voltammetric quantification of O_2

The voltammetric quantification of a range of O_2 contents (% v/v in a flow of N_2) was evaluated at a range of film thicknesses for $[P_{6,6,6,14}][FAP]$ containing 10 mM Fc. It should be noted that Fc was added as an internal reference, in order to normalise the

scans if O_2 content or superoxide accumulation shifted the *quasi*-reference potential. However, over the range of investigated O_2 contents, and despite extensive scanning and use, the formal potential of the Fc/Fc^+ couple was not observed to shift more than *ca.* ±10 mV.

Continuous voltammetric quantification was obtained by continuously cycling between +0.5 V and -1.5 V at 0.1 V s^{-1} while altering the O_2 content. Figure 6 displays selected CVs obtained for a range of O_2 contents at four different RTIL layer thicknesses (Fc redox couple not shown). It can clearly be observed that as the v/v % O_2 increases there is a corresponding increase in the limiting current for O_2 reduction. This is unlikely to correspond to dissolved O_2 (as discussed above, the RTIL layer is too thin to sustain steady state behaviour for O_2) and therefore corresponds to increased flux which is proportional to the O_2 gas content in the gas phase (in the form of the partial pressure, P_{O_2}).

Despite changes in the RTIL layer thickness, the voltammetry for all four systems in Figure 6 is similar. This is particularly true with respect to the steady state current observed for O_2 reduction, such that after extended scanning the different RTIL layer thicknesses were observed to have less of an effect on the steady state current for O_2 reduction than that observed for the individual scans in the equilibrated systems shown Figure 5. This is attributed to stabilisation of the concentration gradients occurring in the system with extended use, with each thickness now possessing relatively similar concentration gradients for O_2 in the RTIL layer.

Figure 7 displays plots for the amperometric responses of the four different

thicknesses with respect to the different O_2 contents shown in Figure 8, by plotting the steady state current observed at -1.50 V for every CV recorded *vs.* the time corresponding to that specific data point. Changes in the O_2 content resulted in clear steps that can be observed in Figure 7, and plots of peak current *vs.* O_2 content (insets in Figure 7) are all linear ($R^2 > 0.995$). This demonstrates the membrane-free microarray system sensitively responds to changes in the oxygen level, producing a linear response over the range of investigated concentrations (*ca.* 2 – 13 % v/v).

Careful analysis of the steady state currents obtained in the two CVs recorded after a change in O_2 content (highlighted in pink in Figure 7, and labeled 1st response and 2nd response in (A)) allows an evaluation of relative response time. A comparison of the current change at the 1st response (*ca.* 18 s after change in O_2 content) and 2nd response (*ca.* 61 s) for the four different film thicknesses is shown in Table 1. A clear improvement in the degree of response *vs.* time is present as the thickness of the RTIL layer is decreased, with all systems displaying some degree of response in less than 18 s.

Figure 8 displays chronoamperometric transients (CA) recorded for a $[P_{6,6,6,14}][FAP]$/Fc film *ca.* 125 μm thick at five different O_2 contents, in order to give more precise data on the response time. This was done by altering the O_2 content 50 s into the CA and monitoring the current response against time.

The response time can be theoretically evaluated as

$$\tau = D / d^2 \qquad (4)$$

where D is the diffusion coefficient of gaseous analyte through the ionic liquid, τ is the response time and d is the thickness of the ionic liquid layer. Using the previously determined diffusion coefficient of O_2 in $[P_{6,6,6,14}][FAP]$ (6.1×10^{-10} m^2 s^{-1} [14]]) the estimated response time is *ca.* 26 s. For all gas concentrations shown in Figure 9, the experimental response time is approximately 29 s and complete equilibration (*e.g.* flat baseline achieved after a change in gas concentration) occurred after *ca.* 100 s.

The 3 s discrepancy between theoretical and experimental values potentially comes from errors in the film thickness, which were estimated based upon the RTIL sitting on the chip as a rectangle, whereas in reality a dome of liquid can be expected above the array. A range of thicknesses are therefore experienced across the array, with the centre of the chip (microelectrode array) experiencing a thicker layer of RTIL than the edge of the chip (counter electrode).

Interestingly, the data in Figure 6 and Table 1 indicate that the response time during continual CV measurement was significantly less than 18 s for all thicknesses. This enhanced response time is attributed to the 'rest period' between scans. During chronoamperometric measurements, the local O_2 concentration is depleted and the analyte therefore has to diffuse the entire thickness of the film (as represented by d in equation (4)). During the CV experiments, the O_2 content is partially regenerated by both oxidation of the superoxide and diffusion of the gas-phase O_2. Therefore, during the next reductive scan after the oxygen content is changed, enough O_2 is present in the RTIL for changes in the P_{O_2} to be detected at the electrode more rapidly due to a

reduced value of *d*. Cyclic voltammetry, or as an alternative pulse voltammetry, are therefore recommended for providing a more rapid qualitative response in this system, while chronoamperometric measurements provide the most rapid quantification (of equilibrated systems) due to steeper concentration gradients.

Thin-layer behaviour

It is anticipated that the thinner the layer of RTIL, the more rapid the response of the sensor. Numerous attempts were made to reduce the thickness of the RTIL below that reported in this paper, for example by spin coating, evaporating dilute solutions of RTIL in non-aqueous solvents, and by physical blotting of the RTIL. While some success was achieved in obtaining Fc electrochemistry consistent with the formation of an extremely thin layer of RTIL on the surface of the array, particularly via blotting, the results have so far been irreproducible, with reduction in layer thickness also uncovering some of the microdiscs as well as removing significant amounts of RTIL from the counter electrode. Work is ongoing in an attempt to optimise the surface properties of the microarray.

CONCLUSIONS

In summary, we have experimentally demonstrated a new oxygen gas sensor that incorporates a room temperature ionic liquid as electrolyte, eliminating the need for a membrane, while also utilising an array of microelectrodes to improve sensitivity. The array significantly enhances the limiting current above that observed for a single

microelectrode. The RTIL $[P_{6,6,6,14}][FAP]$ was chosen for its wetting properties on the microarray, as well as its extreme hydrophobicity. A film of $[P_{6,6,6,14}][FAP]$ 6 µm thick demonstrates <20 s response time and takes *ca.* 1 min to equilibrate (98 % total response) to changes in P_{O_2}, across a range of O_2 contents from *ca.* 2 to 13 v/v %. Such a sensor possesses potential application in more extreme operating conditions, such as high temperature and low pressure, where traditional solvents would volatise but where the RTILs response time is expected to dramatically improve due to lowered viscosity. This study therefore successfully demonstrates the first application of an RTIL/microarray for gas sensing, and reaffirms RTILs to be extremely promising media for the development of high-performance, membrane-less gas sensors.

ACKNOWLEDGEMENTS

X.-J.H. and A.M.O'M thank the EPSRC and Honeywell Analytics for financial support, and J.d.C. acknowledges a Ramón y Cajal Fellowship from the Spanish Ministry of Science and Innovation.

REFERENCES

[1] Wang, J. *Analytical electrochemistry,* 3rd ed., Wiley-VCH: Hoboken, N.J, 2006

[2] http://sensing.honeywell.com [accessed 5th March 2010]

[3] http://www.alphasense.com [accessed 5th March 2010]

[4] http://www.citytech.com [accessed 5th March 2010]

[5] http://www.draeger.com/GC/en/products/detection [accessed 5th March 2010]

[6] Buzzeo, M.C.; Hardacre, C.; Compton, R.G. *Anal. Chem.* **2004**, *76*, 4583-4588

[7] Silvester, D.S.; Compton, R.G. *Z. Phys. Chem.* **2006**, *220*, 1247-1274

[8] Huang, X.J.; Rogers, E.I.; Hardacre, C.; Compton, R.G. *J. Phys. Chem. B* **2009**, *113*, 8953-8959

[9] Buzzeo, M. C.; Klymenko, O. V.; Wadhawan, J. D.; Hardacre, C.; Seddon, K. R.; Compton, R. G.; *J. Phys. Chem. A* **2003**, *107*, 8872– 8878

[10] Barnes, A. S.; Rogers, E. I.; Streeter, I.; Aldous, L.; Hardacre, C.; Wildgoose, G. G.; Compton, R. G. *J. Phys. Chem. C* **2008**, *112*, 13709– 13715

[11] Rogers, E.I.; Huang, X.J.; Dickinson, E.J.F.; Hardacre, C.; Compton, R.G. *J. Phys. Chem. C* **2009**, *113,* 17811–17823

[12] Carter, M. T.; Hussey, C. L.; Strubinger, S. K. D.; Osteryoung, R. A. *Inorg. Chem.* **1991**, *30*, 1147– 1151

[13] Islam, M. M.; Ohsaka, T. *J. Phys. Chem. C* **2008**, *112*, 1269– 1275

[14] Evans, R. G.; Klymenko, O. V.; Saddoughi, S. A.; Hardacre, C.; Compton, R. G. *J. Phys. Chem. B* **2004**, *108,* 7878– 7886

[15] Zhang, D.; Okajima, T.; Matsumoto, F.; Ohsaka, T. *J. Phys. Chem. B* **2004**, *151,* D31–

D37

[16] Katayama, Y.; Onodera, H.; Yamagata, M.; Muira, T. *J. Electrochem. Soc.* **2004**, *151*, A59– A63

[17] Al Nashef, I.M.; Leonard, M.L.; Kittle, M.C.; Matthews, M.A.; Weidner, J. W. *Electrochem. Solid-State Lett.* **2001**, *4*, D16– D18

[18] Villagran, C.; Aldous, L.; Lagunas, M.C.; Compton, R.G.; Hardacre, C. *J. Electroanal. Chem.* **2006**, *588*, 27-31

[19] Rene, A.; Hauchard, D.; Lagrost, C.; Hapiot, P. *J. Phys. Chem. B* **2009**, *113*, 2826-2831

[20] Huang, X.J.; O'Mahony, A.M.; Compton, R.G. *Small* **2009**, *5*, 776-788

[21] Wang, R.; Hoyano, S.; Ohsaka, T. *Chem. Lett.* **2004**, *33*, 6

[22] Wang, R.; Okajima, T.; Kitamura, F.; Ohsaka, T. *Electroanalysis* **2004**, *16*, 66

[23] Jin, X.; Yu, L.; Garcia, D.; Ren, R.X.; Zeng, X. *Anal. Chem.*, **2006**, *78*(19), 6980–6989

[24] Toniolo, R.; Pizzariello, A.; Susmel, S.; Dossi, N.; Doherty, A.P.; Bontempelli, G. *Electroanalysis*, **2007**, *19*, 2141-2148

[25] Yu, L.; Huang, Y.; Jin, X.; Mason, A.J.; Zeng, X. *Sens. Actuators, B: Chem*., **2009**, *140*, 363-370

[26] O'Mahony, A.M.; Silvester, D.S.; Aldous, L.; Hardacre, C.; Compton, R.G. *J. Chem. Eng. Data* **2008**, *53*, 2884-2891.

[27] Menshykau, D.; O'Mahony, A. M.; Del Campo, F. J.; Munoz, F. J.; Compton, R. G., *Anal. Chem.* **2009**, *81*(22), 9372–9382.

[28] Ignat'ev, N.V.; Welz-Biermann, U.; Kucheryna, A.; Bissky G.; Willner, H.; *J. Fluorine*

Chem. **2005**, *126*, 1150–1159

[29] Buzzeo, M.C.; Hardacre, C.; Compton, R.G. *ChemPhysChem* **2006**, *7*, 176-180.

[30] Dyson, P.J.; Laurenczy, G.; Ohlin, C.A.; Vallance J.; Welton T. *Chem. Commun.* **2003**, 2418-2419

[31] Rogers, E.I.; Silvester, D.S.; Poole, D.L.; Aldous, L.; Hardacre, C.; Compton, R.G. *J. Phys. Chem. C* **2008**, *112*, 2729-2735

[32] Bard, A.J.; Faulker, L.R. *Electrochemical Methods*, 2nd ed.; Wiley: New York, 2001.

[33] Barrosse-Antle, L.E.; Aldous, L.; Hardacre, C.; Bond, A.M.; Compton, R.G. *J. Phys. Chem. C* **2009**, *113*, 7750-7754

[34] Vorotyntsev, M.A.; Zinovyeva, V.A.; Konev, D.V.; Picquet, M.; Gaillon, L.; Rizzi, C. *J. Phys. Chem. B* **2009**, *113* (4), 1085–1099

[35] Emel'yanenko, V.N.; Verevkin, S.P.; Krol, O.V.; Varushchenko R.M.; Chelovskaya, N.V. *J. Chem. Thermodyn.* **2007**, *39*(4), 594-601

Figure Captions:

Figure 1. A) Schematic diagrams outlining the fabrication process for creating recessed Au microdisc array using photolithography. B) Mask types.

Figure 2. Recessed microdisc array. A) General layout of a chip containing recessed microdisc array. Connector 1 leads to a large auxiliary electrode (CE); Connector 2 leads to the array of microdiscs (WE); Connector 3 is a smaller auxiliary for use as pseudo-reference (RE); Connector 4 corresponds to an array of microrings (not used in this work). B) Optical microscopy image, face-on view, showing a representative section of the array. C) Confocal microscopy image of individual electrode in an array, clearly showing a recessed disc feature. D) Cross section of individual recessed electrode in confocal image (scan following the white dotted line in panel C). The diameter is shown to be approximately 12 μm.

Figure 3. Typical cyclic voltammetry for the reduction of oxygen in 0.2 μl $[P_{6,6,6,14}][FAP]$ in 3.5% O_2 / 96.5% N_2 gas mixture on the Au microdisc array at a scan rate of 0.1 V s^{-1}. The thickness of 0.2 μl $[P_{6,6,6,14}][FAP]$ was calculated as 12.5 μm assuming its volume is cubic on the chip surface. The dotted line shows a blank scan under 100% N_2. The arrows show the direction of the scan. The inset is a diagram of a membrane-free amperometric gas sensor. In this case the electrolyte is a non-volatile RTIL while the analyte is an O_2/N_2 gas mixture.

Figure 4. Typical cyclic voltammograms at a range of scan rates (0.1, 0.4, and 1 V s^{-1}) for the reduction of oxygen in 2 μl $[P_{6,6,6,14}][FAP]$/Fc in 2.3% O_2 / 97.7% N_2 gas mixture on a chip containing recessed Au microdisc array. The thickness of 2 μl

$[P_{6,6,6,14}][FAP]$ was calculated as 125 μm. The inset displays an illustration of the dominant diffusion processes for O_2, corresponding to steady state diffusion at slow scan rates and transient diffusion at high scan rates.

Figure 5. Typical cyclic voltammograms for differing $[P_{6,6,6,14}][FAP]$ film thicknesses (6, 30, 95, and 125 μm) for the reduction of oxygen in a 2.3% O_2 / 97.7% N_2 gas mixture on the Au microdisc array. Scan rate: 0.1 V s^{-1}. The different film thicknesses corresponds to 0.1, 0.5, 1.5, and 2 μl $[P_{6,6,6,14}][FAP]$, respectively. The observed trends are rationalised in the text.

Figure 6. Typical cyclic voltammograms (scan rate 0.1 V s^{-1}) at different film thicknesses of $[P_{6,6,6,14}][FAP]$ for the reduction of oxygen in varying volume % O_2 on the Au microdisc array. (A) 6 μm; (B) 12.5 μm; (C) 30 μm; (D) 125 μm.

Figure 7. Current-time recording obtained at the recessed microdisc array which is covered by different thicknesses of $[P_{6,6,6,14}][FAP]$. (A) 6 μm; (B) 12.5 μm; (C) 30 μm; (D) 125 μm. Data was collected from continuous CVs (scan rate 0.1 V s^{-1}) at varying % v/v O_2 (corresponding to those shown in Figure 6). The inset in panel A, B, C, and D shows the plot of current as a function of volume % O_2, respectively, with linear trendlines ($R^2 > 0.995$ for all).

Figure 8. Potential step chronoamperometric transient for the reduction of O_2 in 2 μl $[P_{6,6,6,14}][FAP]$ on a recessed microdisc array. The potential was jumped from 0.0 V to -1.50 V at t = 0 s. One gas concentration was maintained for t = 0 to 50 s, then increased for t = 50 to 250 s. The v/v % O_2 contents in N_2 are (1) 1.96 to 3.66 %; (2) 3.66 to 5.12 %; (3) 5.12 to 7.41 %; (4) 7.41 to 8.26 %; (5) 8.26 to 9.91 %; (6) 9.91 to

11.03 %.

Table 1. Percentage of Total Response at the Recessed Microdisc Array with different thicknesses (*d*) of [$P_{6,6,6,14}$][FAP]

[$P_{6,6,6,14}$][FAP]		Steady-State Current / nA		Total Response (%) at	
V / µl	*d* / µm	at Low Conc.	at High Conc.	1st scan (*ca.* 18 s)	2nd (*ca.* 61 s)
2.0	125	-38.6	-45.2	21	70
0.5	31.3	-27.5	-34.8	56	89
0.2	12.5	-33.5	-40.6	63	92
0.1	6	-32.5	39.1	79	98

Percentage of total response is given by $(I_{1st} - I_{Low\ Conc.})/(I_{High\ Conc.} - I_{Low\ Conc.})$ and $(I_{2nd} - I_{Low\ Conc.})/(I_{High\ Conc.} - I_{Low\ Conc.})$

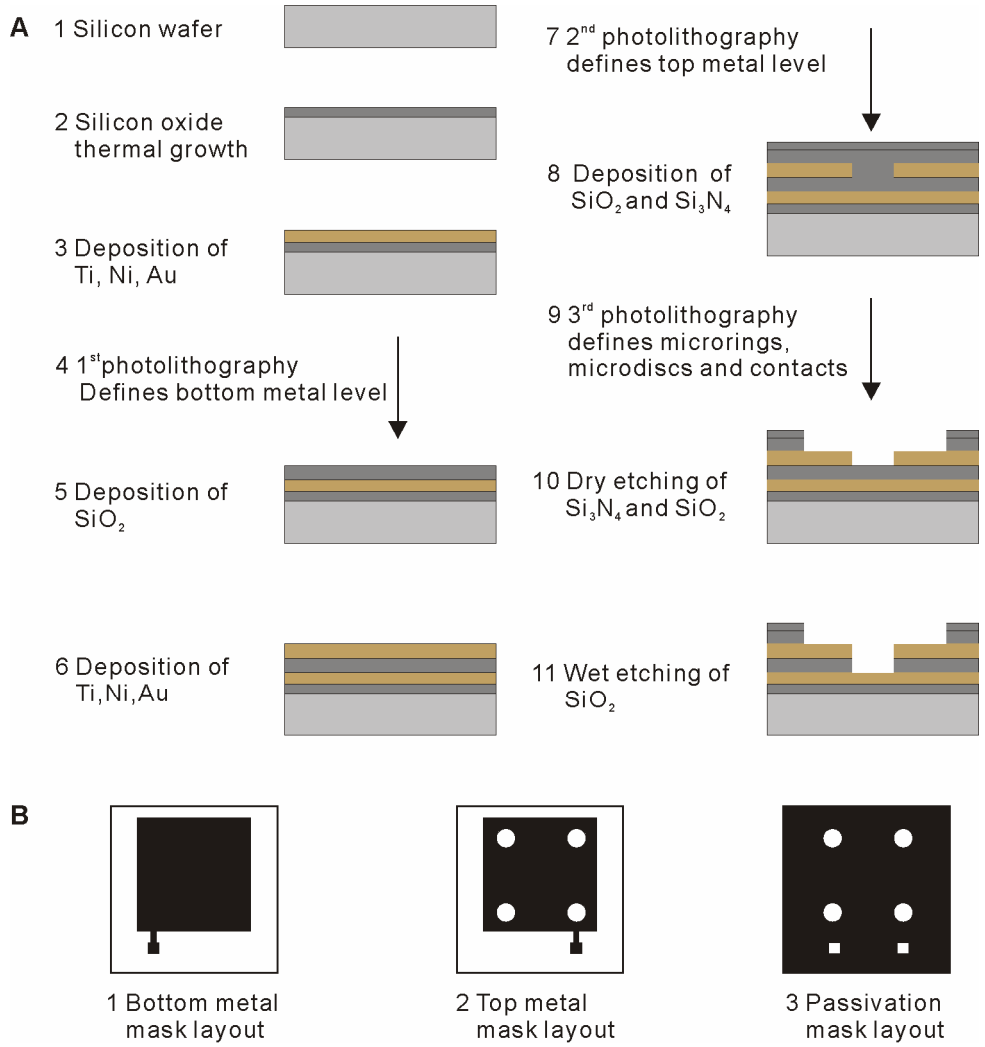

Figure 1. A) Schematic diagrams outlining the fabrication process for creating recessed Au microdisc array using photolithography. B) Mask types.

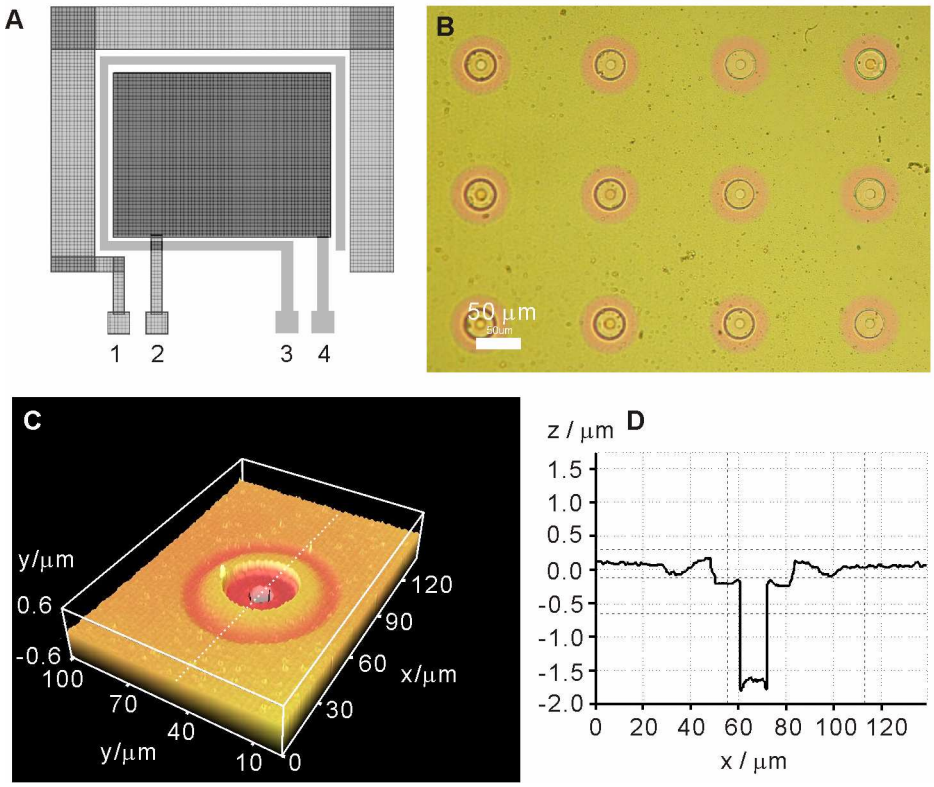

Figure 2. Recessed microdisc array. A) General layout of a chip containing recessed microdisc array. Connector 1 leads to a large auxiliary electrode (CE); Connector 2 leads to the array of microdiscs (WE); Connector 3 is a smaller auxiliary for use as pseudo-reference (RE); Connector 4 corresponds to an array of microrings (not used in this work). B) Optical microscopy image, face-on view, showing a representative section of the array. C) Confocal microscopy image of individual electrode in an array, clearly showing a recessed disc feature. D) Cross section of individual recessed electrode in confocal image (scan following the white dotted line in panel *C*). The diameter is shown to be approximately 12 µm.

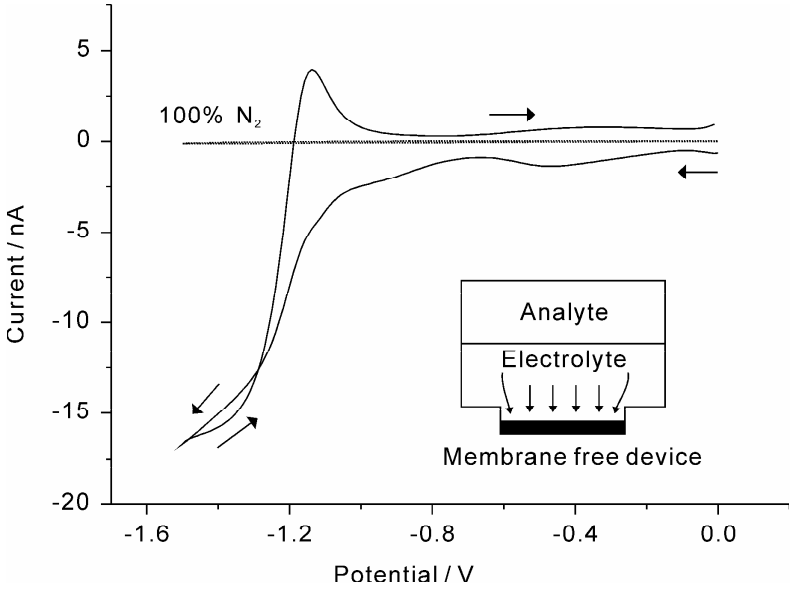

Figure 3. Typical cyclic voltammetry for the reduction of oxygen in 0.2 µl $[P_{6,6,6,14}][FAP]$ in 3.5% O_2 / 96.5% N_2 gas mixture on the Au microdisc array at a scan rate of 0.1 V s^{-1}. The thickness of 0.2 µl $[P_{6,6,6,14}][FAP]$ was calculated as 12.5 µm assuming its volume is cubic on the chip surface. The dotted line shows a blank scan under 100% N_2. The arrows show the direction of the scan. The inset is a diagram of a membrane-free amperometric gas sensor. In this case the electrolyte is a non-volatile RTIL while the analyte is an O_2/N_2 gas mixture.

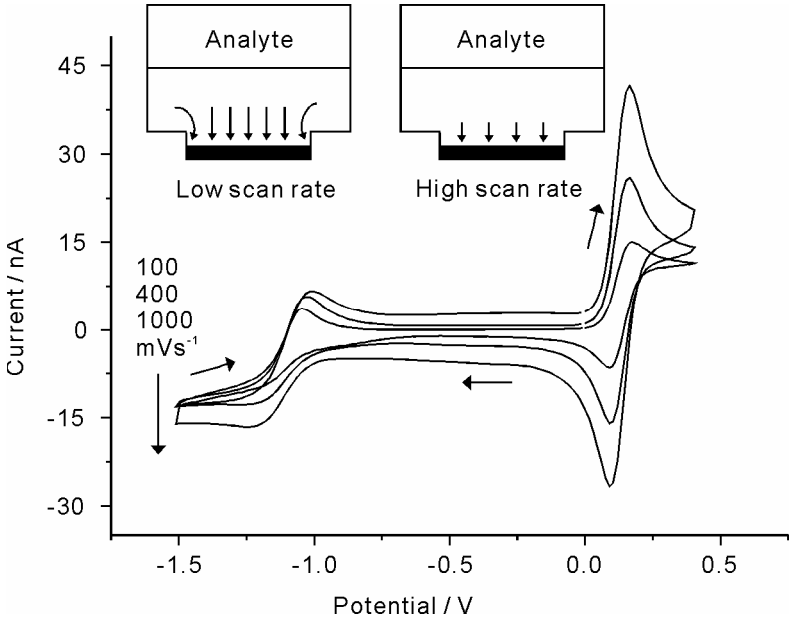

Figure 4. Typical cyclic voltammograms at a range of scan rates (0.1, 0.4, and 1 V s^{-1}) for the reduction of oxygen in 2 µl $[P_{6,6,6,14}][FAP]$/Fc in 2.3% O_2 97.7% N_2 gas mixture on a chip containing recessed Au microdisc array. The thickness of 2 µl $[P_{6,6,6,14}][FAP]$ was calculated as 125 µm. The inset displays an illustration of the dominant diffusion processes for O_2, corresponding to steady state diffusion at slow scan rates and transient diffusion at high scan rates.

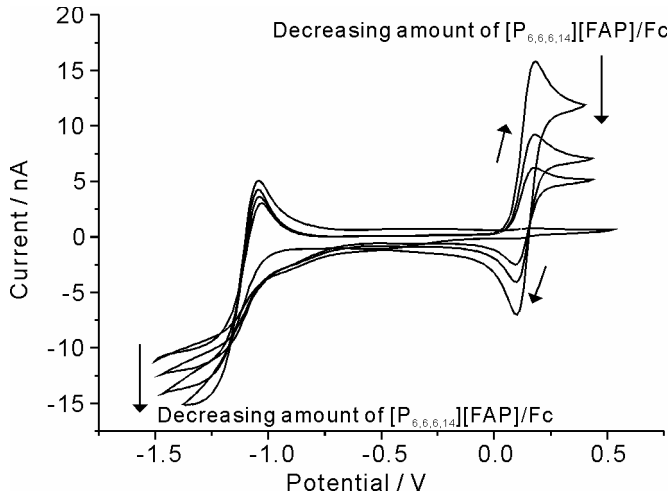

Figure 5. Typical cyclic voltammograms for differing $[P_{6,6,6,14}][FAP]$ film thicknesses (6, 30, 95, and 125 μm) for the reduction of oxygen in a 2.3% O_2 / 97.7% N_2 gas mixture on the Au microdisc array. Scan rate: 0.1 V s^{-1}. The different film thicknesses corresponds to 0.1, 0.5, 1.5, and 2 μl $[P_{6,6,6,14}][FAP]$, respectively. The observed trends are rationalised in the text.

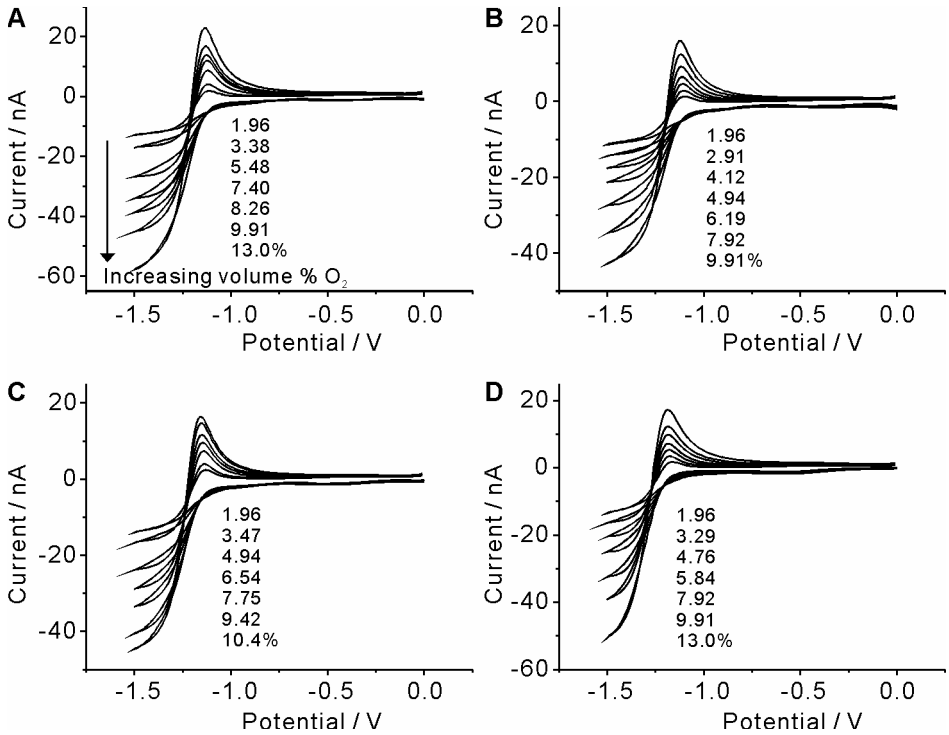

Figure 6. Typical cyclic voltammograms (scan rate 0.1 V s^{-1}) at different film thicknesses of $[P_{6,6,6,14}][FAP]$ for the reduction of oxygen on the Au microdisc array at various v/v % O_2. (A) 6 μm; (B) 12.5 μm; (C) 30 μm; (D) 125 μm.

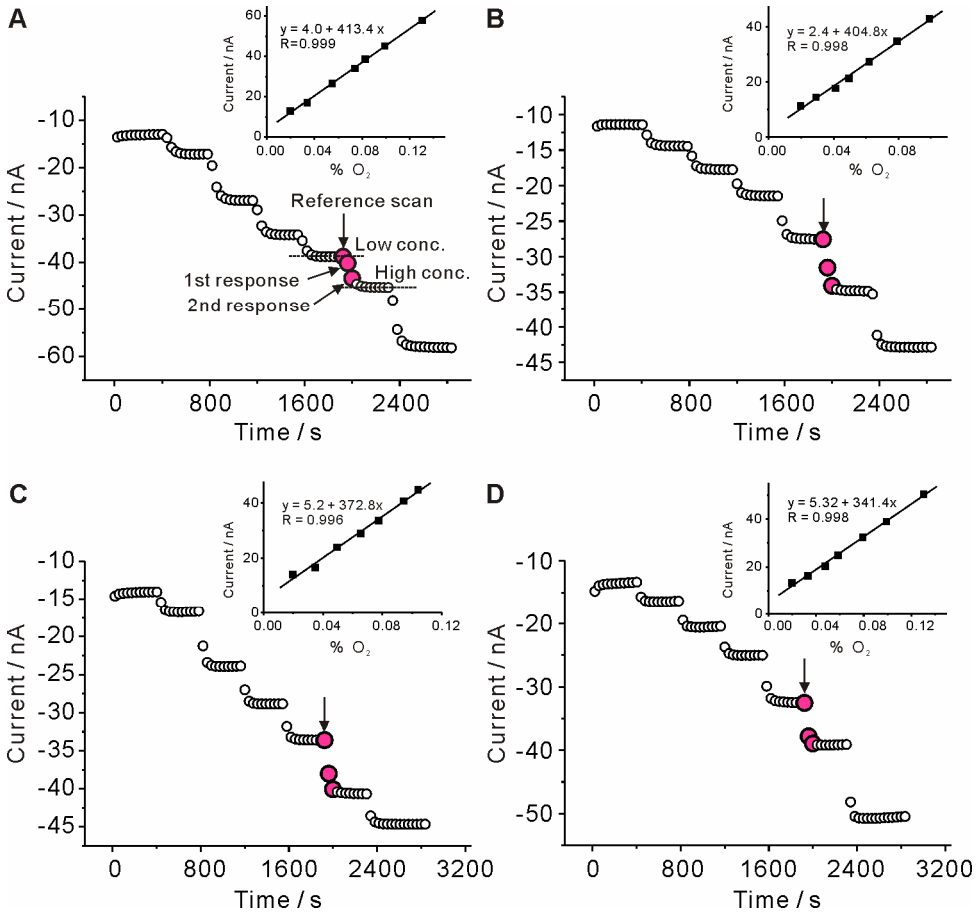

Figure 7. Current-time recording obtained at the recessed microdisc array which is covered by different thicknesses of $[P_{6,6,6,14}][FAP]$. (A) 125 µm; (B) 30 µm; (C) 12.5 µm; (D) 6 µm. Data was collected from continuous CVs (scan rate 0.1 V s^{-1}) at varying % v/v O_2 (corresponding to those shown in Figure 6). The inset in panel A, B, C, and D shows the plot of current as a function of volume % O_2, respectively, with linear trendlines ($R^2 > 0.995$ for all).

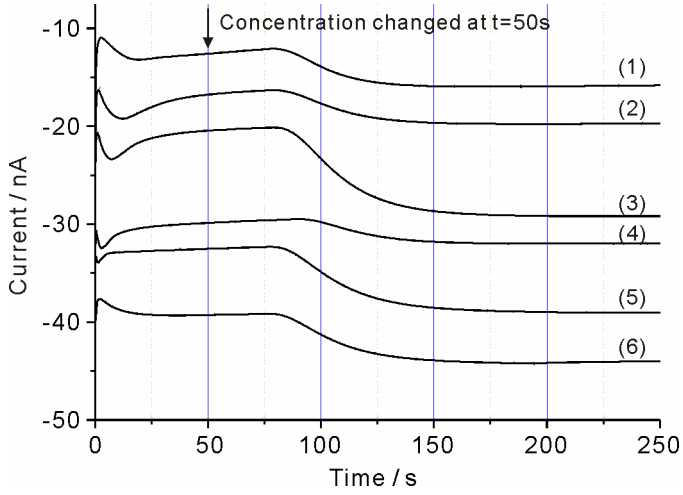

Figure 8. Potential step chronoamperometric transient for the reduction of O_2 in 2 µl $[P_{6,6,6,14}][FAP]$ on a recessed microdisc array. The potential was jumped from 0.0 V to -1.50 V at t = 0 s. One gas concentration was maintained for t = 0 to 50 s, then increased for t = 50 to 250 s. The v/v % O_2 contents in N_2 are (1) 1.96 to 3.66 %; (2) 3.66 to 5.12 %; (3) 5.12 to 7.41 %; (4) 7.41 to 8.26 %; (5) 8.26 to 9.91 %; (6) 9.91 to 11.03 %.

End